An Event-Based Approach to Explore Selected Present and Future Atmospheric River–Induced Floods in Western Norway

TRINE J. HEGDAHL

Norwegian Water Resources and Energy Directorate, Oslo, Norway

KOLBJØRN ENGELAND

Norwegian Water Resources and Energy Directorate, and University of Oslo, Oslo, Norway

MALTE MÜLLER

Norwegian Meteorological Institute, Oslo, Norway

JANA SILLMANN

Center for International Climate Research, Oslo, Norway

(Manuscript received 29 March 2019, in final form 30 April 2020)

ABSTRACT

The aim of this study is to investigate extreme precipitation events caused by atmospheric rivers and compare their flood impact in a warmer climate to current climate using an event-based storyline approach. The study was set up by selecting four high-precipitation events from 30 years of present and future climate simulations of the high-resolution global climate model EC-Earth. The two most extreme precipitation events within the selection area for the present and future climate were identified, and EC-Earth was rerun creating 10 perturbed realizations for each event. All realizations were further downscaled with the regional weather prediction model, AROME-MetCoOp. The events were thereafter used as input to the operational Norwegian flood-forecasting model for 37 selected catchments in western Norway, and the magnitude and the spatial pattern of floods were analyzed. The role of the hydrological initial conditions, which are important for the total flooding, were analyzed with a special emphasis on snow and soil moisture excess. The results show that the selected future extreme precipitation events affected more catchments with larger floods, compared to the events from present climate. In addition, multiple realizations of the meteorological forcing and four different hydrological initial conditions, for example, soil saturation and snow storage, were important for the estimation of the maximum flood level. The meteorological forcing (e.g., the internal variability/perturbed output) accounts for the highest contribution to the spread in flood magnitude; however, for some events and catchments the hydrological initial conditions affected the magnitudes of floods more than the meteorological forcing.

1. Introduction

Atmospheric rivers are transient, narrow routes of water vapor supplying a substantial fraction of the moisture transport from tropical or extratropical latitudes toward the poles (Zhu and Newell 1998; Ralph and Dettinger 2011; Ralph et al. 2017). When such air

masses with a high moisture content reach a topographical barrier like the west coast of Norway, the air parcels are lifted and adiabatically cooled, forming clouds and precipitation (Stohl et al. 2008). For western Norway, the most extreme precipitation, flood, and landslide events since 1900 can largely be attributed to atmospheric rivers (Stohl et al. 2008; Lavers and Villarini 2013, 2015; Azad and Sorteberg 2017; Benedict et al. 2019). Three recent examples of atmospheric rivers unfolded and affected western Norway quite differently. In September 2005, an atmospheric river hit the city of Bergen, with a precipitation intensity that was record

---

ⓐ Denotes content that is immediately available upon publication as open access.

Corresponding author: Trine J. Hegdahl, tjh@nve.no

high, and measured to 156.5 mm $(24\,h)^{-1}$ and 111 mm $(12\,h)^{-1}$ (Iden et al. 2005; Stohl et al. 2008). The precipitation intensity triggered landslides and floods causing locally large damages and casualties. In October 2014, high precipitation of long duration, which coincided with initially high groundwater and soil moisture content, caused large floods in multiple catchments (Langsholt et al. 2015). In October 2018, a cold period allowing snow to accumulate at high altitudes was followed by a very warm atmospheric river event. The combination of rainfall and extensive snowmelt caused floods and large damages, affecting areas not usually susceptible to autumn floods (Vannforeningen 2018). These examples of atmospheric river induced floods demonstrate that a combination of several factors contribute to the total flood impact: the nature of the atmospheric river event itself, including moisture content, landfall, dynamic development, precipitation intensity and duration, as well as the antecedent weather that defines the hydrological initial conditions. Due to the important contribution from snowmelt and the initial soil moisture, there is no unique relationship between precipitation intensities or volumes and flood sizes (Berghuijs et al. 2019).

In the present climate, the Norwegian west coast is one of the wettest parts of Europe with annual precipitation of more than 3000 mm (Stohl et al. 2008). Rain is the major contributor to floods, whereas the contribution from snowmelt increases with elevation and distance from the coast (Kobierska et al. 2018). The majority of and the largest flood events in this region occur in the autumn or early winter (Roald 2008), which overlaps with the main seasons for atmospheric rivers (Azad and Sorteberg 2017). Climate projections for western Norway indicate increased precipitation in the future, where both the number of days with intense rainfall and the intensity of the rainfall will increase (Caroletti and Barstad 2010; Hanssen-Bauer et al. 2017). Baatsen et al. (2015) show that the changes in diabatic heating and moisture transport due to a warmer Atlantic Ocean will cause more severe storms over western Europe and affect storm paths. Storms hitting the British Isles today might move more toward Scandinavia in the future.

To investigate future climate extreme precipitation and floods, often an ensemble of climate models is used to obtain probabilities for future extremes (e.g., Sillmann et al. 2013; Hanssen-Bauer et al. 2017). The standard approach is to apply a climate–hydrological modeling chain that includes an ensemble of global climate models (GCMs), regional climate models (RCMs), and/or statistical downscaling methods, and hydrological models (Olsson et al. 2016). For instance, Lawrence and Hisdal (2011) and Lawrence (2016) estimate the flood probabilities and frequencies for Norwegian rivers based on continuous simulations from such ensembles. Several studies show that the floods in western Norway will increase due to increased future precipitation, and shift toward more rain-induced floods in autumn and winter (e.g., Sorteberg et al. 2018; Hanssen-Bauer et al. 2017; Vormoor et al. 2016; Lawrence and Hisdal 2011).

For Norway, the information extracted from the climate projection studies guides the societal adaptation strategies. The projection studies are the basis for tailored guidelines for climate adaptation for communities (http://www.klimatilpasning.no/infosider/english/), provided by the Norwegian Center for Climate Services (https://klimaservicesenter.no/). One example of a current practice is the use of flood inundation maps that include estimated future flood levels for specific return periods, based on the expected change in streamflow (e.g., Orvedal and Peereboom 2014; https://gis3.nve.no/link/?link=flomsone). The flood inundation maps indicate the water level during a 200-yr flood in a future climate, and these maps are hence the basis for land-use planning and govern the placement of buildings and important infrastructure to avoid future flooding. In addition, the future climate is important for the hydropower industry in Norway, both in terms of dam safety and water available for electricity production.

For most purposes, a multimodel GCM modeling approach is favored. There are, however, instances where one or few models are preferable (IPCC 2010). Some GCMs might resolve and describe specific weather processes better than other GCMs. An example of a weather process that is better described by higher-resolution GCM is the landfall of atmospheric rivers causing orographic precipitation over western Norway. For atmospheric rivers, the model description of the topographical barrier is of the utmost importance to get well-represented precipitation by mountains (Neiman et al. 2009). Large errors might arise in a steep terrain where the elevation and hence precipitation varies greatly, especially for small catchments where the area is smaller than the grid resolution of a GCM. In a future climate, more atmospheric rivers will make landfall while temperatures are above the freezing point, and thereby deposit less snow and more rain due to higher mean temperature (Whan et al. 2020) and hence influence the seasonality of atmospheric river induced floods. While atmospheric rivers and their future changes have garnered recent attention in climate studies (e.g., Dettinger 2011; Ralph and Dettinger 2011; Espinoza et al. 2018), their ultimate effect on catchment-level flows is not as well studied.
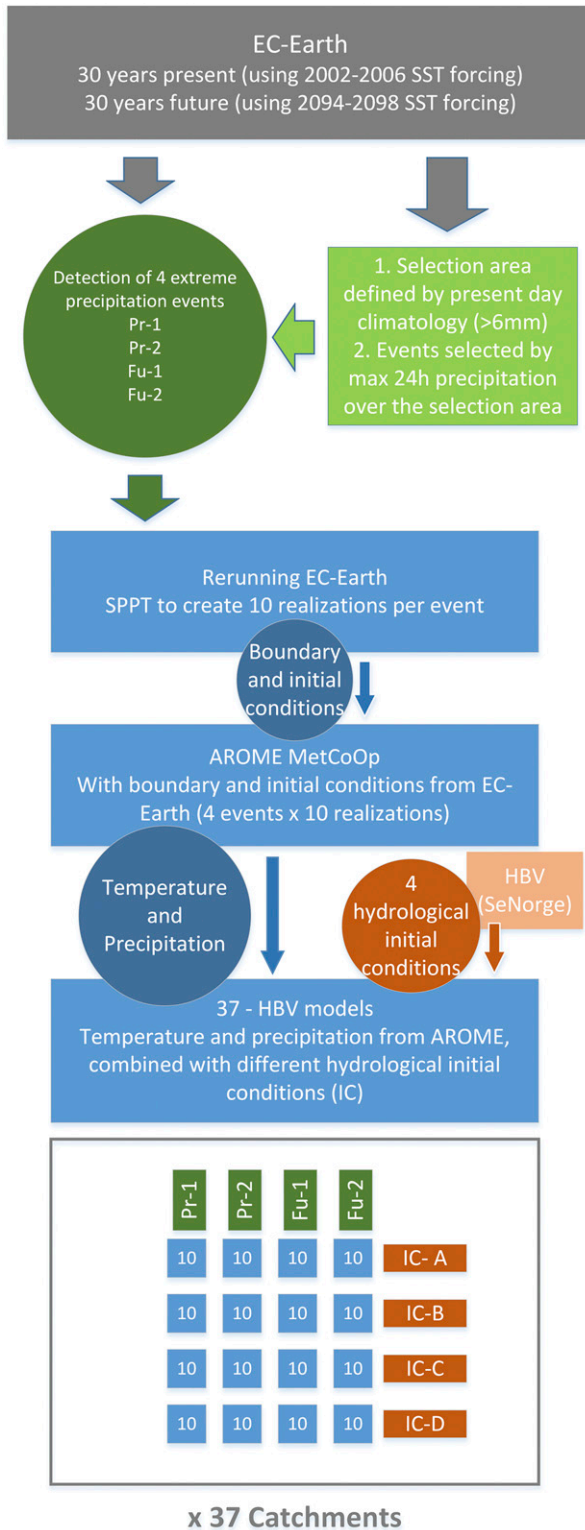
FIG. 1. The processing chain starting from EC-Earth climate projections, using SST forcing (Hazeleger et al. 2010; Haarsma et al. 2013). Further describing the event selections where the maximum 24-h precipitation over western Norway is chosen. For each event, stochastic perturbation of physical tendencies (SPPT)

The aim of this study is to analyze the impact of extreme atmospheric river events in western Norway under present and future climate by using an event-based storyline approach as outlined in Hazeleger et al. (2015). Shepherd et al. (2018) defines a storyline as "a physical self-consistent unfolding of past events, or of possible future events or pathways." Moreover, Shepherd et al. (2018) argue that one reason for applying a storyline approach is to improve awareness of risk based on plausibility rather than probability. The storyline approach is particularly useful for decision makers since it enables them to assess "impact of particular actions under an uncertain regional climate change" (Shepherd 2019). By applying an event-based storyline approach and selecting only a few events, it is easier to do more computer-intensive high-resolution global and regional modeling than is possible with a coarse resolution multi-model ensemble of GCMs. High-resolution climate modeling is important for our study area with complex topography that is not captured in coarse resolution GCMs (Prein et al. 2015). The latter will often result in large precipitation and/or temperature biases that would need correction before being used as input for, for example, hydrological impact modeling (e.g., Maraun 2016). In this study, we used a modeling chain similar to the operational flood-forecasting modeling chain, and thereby familiar to stakeholders in Norway. By using a familiar modeling chain, established exceedance thresholds, and warning colors, it is easier to assess implications of future floods and it facilitates the communication about future flood impact and risk awareness. The comprehension and utilization of climate change data depend on the user (Porter and Dessai 2017; Howarth et al. 2017), and there is often a mismatch between the scientist perception of what the user need and what the user wants. We believe that the approach used in this study is a contribution to mitigating this mismatch.

The event-based storyline approach used for this study comprises the entire modeling chain from a high-resolution global climate model, to a regional weather prediction model and finally a hydrological model estimating floods (Fig. 1). A novel aspect is that the two

←

is used to establish new event realizations by rerunning EC-Earth. All EC-Earth realizations are downscaled using the regional weather forecasting model AROME-MetCoOp. Temperature and precipitation data from AROME-MetCoOp are the input to the hydrological models (HBV), which are run for all selected events in combination with four different hydrological initial conditions. The hydrological initial conditions are determined by running HBV with seNorge-interpolated observational data.

downstream models are similar to the operational weather and flood-forecasting models, and thus optimally calibrated to the region of interest. Further, the global climate model has a spatial resolution comparable to that of the global weather prediction model used operationally. With this model setup, we investigated atmospheric river driven extreme precipitation events for western Norway under present and future climates. In addition to the change in precipitation magnitude and intensity in a future climate, the hydrological initial conditions might also change, and should be addressed more specifically (e.g., Sharma et al. 2018). We therefore selected a set of four different characteristic initial conditions that we combined with all atmospheric river events. The hydrological initial conditions were established using historical data from selected years to spin up the hydrological model. This approach enabled us to consider the importance of the hydrological initial states when we wanted to represent different future flood scenarios. Furthermore, we highlighted different flood responses to the atmospheric river events and evaluated the relative importance of hydrological initial conditions and multiple meteorological model realizations on the flood estimations.

2. Models and methods

a. Global climate model

We used simulations from the global climate model EC-Earth v2.3 (Hazeleger et al. 2010; Haarsma et al. 2013) with a resolution of about 25 km (T799L91). High-resolution global climate models with spatial resolutions of around 30 km are better capable of simulating the water transport over the Atlantic compared to coarse resolution global models, and hence can better represent small-scale extreme weather systems (Haarsma et al. 2013). Two different model ensemble simulations were considered, a present-day scenario from 2002 to 2006 and a future scenario from 2094 to 2098. Each scenario consists of an ensemble of six independent members, for which the initial atmospheric conditions are determined by running a low-resolution model (EC-Earth, T159) 10 years, and use one of the first six days after the spinup period as atmospheric conditions for each of the six ensemble members. The EC-Earth model (T799L91) is run for 3 months, to ensure that the members are independent. Thereafter, the six independent members are run for 5 years starting 1 January, which for each period results in a 30-yr dataset. In the present-day simulations, observed greenhouse gas and aerosol concentrations are applied, while in the future simulation the concentrations are derived from the representative concentration pathway (RCP) 4.5 scenario (van Vuuren et al. 2011).

The sea surface temperatures (SSTs) are used as lower boundary condition. For the period from 2002 to 2006, a daily SST satellite product (http://www.ncdc.noaa.gov/oa/climate/research/sst/oi-daily.php) is used. For the period from 2094 to 2098, the ensemble mean changes in SST from future projections of a coupled atmosphere–ocean climate model using the SRES A1B scenario (ESSENCE project; Sterl et al. 2008; Haarsma et al. 2013) is added to the 2002–06 SST. The projected global temperature change at the end of the century under SRES A1B lies within the CMIP5-projected range under RCP4.5 (Sillmann et al. 2013).

Haarsma et al. (2013) provide a detailed description of the EC-Earth model setup. The EC-Earth simulations are previously used and validated in several studies (e.g., van der Linden et al. 2018; van Haren et al. 2015; Bintanja et al. 2014; Baatsen et al. 2015; Haarsma et al. 2013). Further, Whan et al. (2020) show that the present EC-Earth simulations, when compared to ERA-Interim (Dee et al. 2011), are able to represent both the frequency and intensity of atmospheric river precipitation in present climate. The integrated water vapor transport (IVT) is a measure used to track and define the atmospheric rivers. Whan et al. (2020) used an automatic algorithm to track the atmospheric rivers from 6-hourly integrated water vapor transport and defined the IVT exceedance threshold for the present climate period to $368 \, kg \, m^{-1} \, s^{-1}$ (95% percentile). In Fig. 2, we find that the 98% percentile of the IVT in EC-Earth is similar to ERA-Interim, which confirms that results from EC-Earth can be used to identify atmospheric rivers.

b. Event selections

Since nearly all large-scale precipitation extremes at the west coast of Norway are connected to atmospheric rivers (Lavers and Villarini 2015; Azad and Sorteberg 2017; Benedict et al. 2019), the events were selected by identifying the two largest daily precipitation values in a predefined area. The spatial pattern of precipitation is to a large degree controlled by orographic mechanisms. Therefore, the area used to select the events was defined by grid cells where the EC-Earth simulated extreme precipitation, constrained within 57.1°–63.2°N and 2.6°–9.3°E, derived from the 30-yr present-day climatology, exceeded an average of 6 mm day^{-1}. The grid cells used in the selection of events for western Norway are shown as a gray shaded area in Fig. 3. The two most extreme precipitation events within the selection area for the present and future climates were identified. From a 30-yr daily dataset, the two highest daily values represent the 99.98% percentile. The two present climate EC-Earth events had a daily average precipitation over the selection area of 84 and 74 mm day^{-1}, whereas the

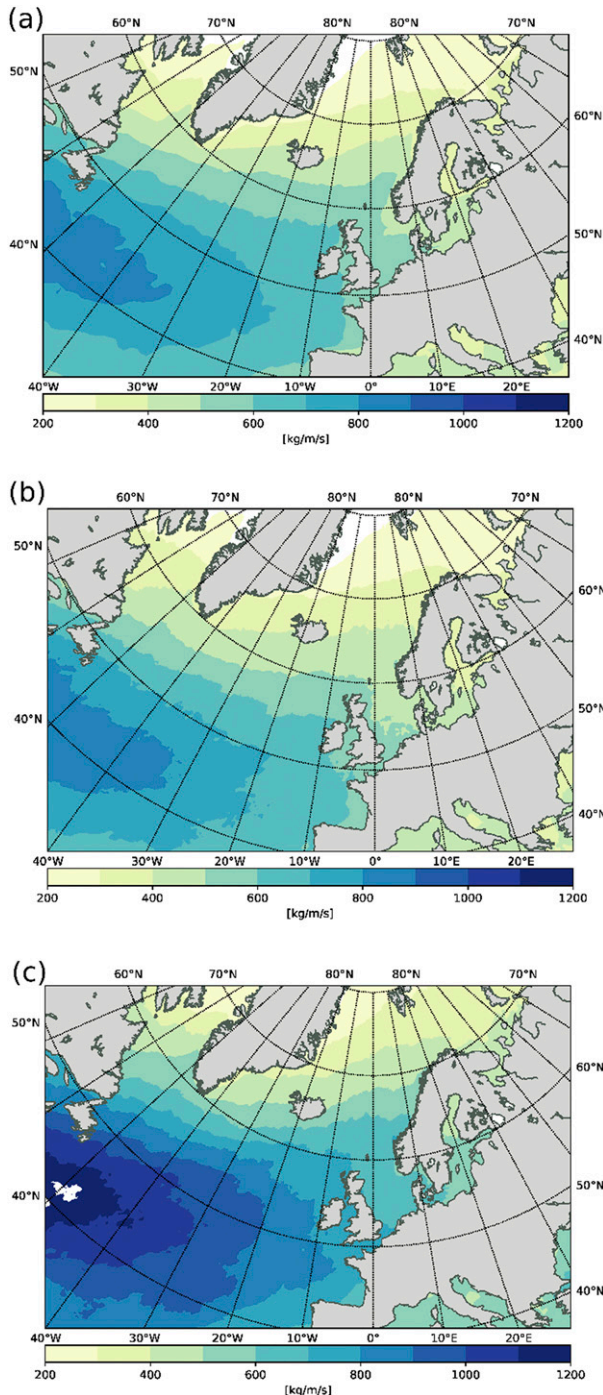FIG. 2. The 98% percentile of the daily mean IVT ($kg\,m^{-1}\,s^{-1}$) for (a) ERA-Interim 1976–2016, (b) 30 years of EC-Earth present day, and (c) 30 years of EC-Earth future are shown.
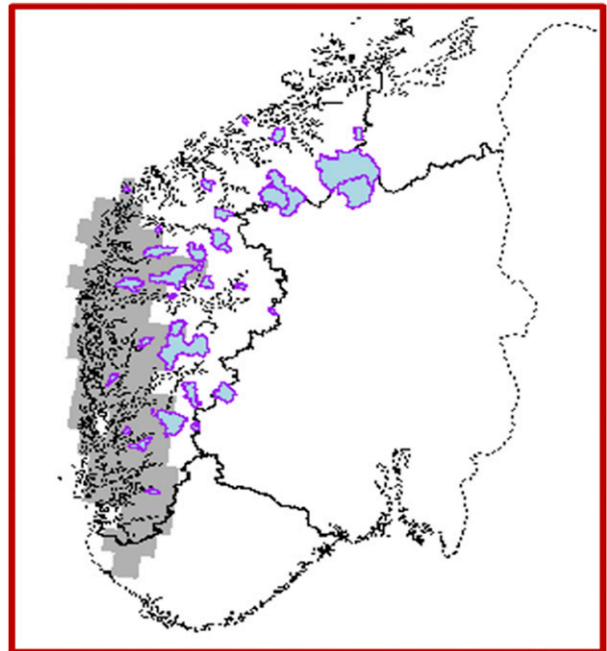

FIG. 3. The gray shaded area defines grid cells in the EC-Earth model used to select the atmospheric river events over the west coast of Norway, whereas the location and catchment area of the 37 catchments are marked in blue with a pink outline. The red box in Fig. 4 defines the extent of this map.

future events had daily average precipitation of 94 and 92 mm day^{-1}.

A visual inspection of the IVT patterns of the selected events confirmed the initial assumption that the events were caused by atmospheric rivers, shown as the strong filaments of IVT originating in the Atlantic (Fig. 4). For each selected event, 10 alternative realizations were generated in EC-Earth by stochastically perturbing the model physics tendencies (SPPT) 5 days prior to the selected event in EC-Earth. The SPPT method is similar to that used for the operational ensemble forecasting at the European Centre for Medium-Range Weather Forecasts (ECMWF; Persson 2015).

c. Regional model

To obtain more realistic values of extreme precipitation, AROME-MetCoOp a nonhydrostatic weather forecasting system (Müller et al. 2017), was utilized for downscaling the 4 × 10 realizations from EC-Earth. AROME-MetCoOp is the operational weather forecasting system for Norway, Sweden and Finland (domain defined in Fig. 4) and is used as input for the operational hydrological forecasting systems in Norway. The AROME-MetCoOp model has a spatial resolution of 2.5 km and is initialized and forced at the lateral boundaries by ECMWF IFS in the operational setup, which was replaced by the EC-Earth realizations for this model setup. The simulations were initiated 36 h before the extreme event and simulated over a period of 144 h.

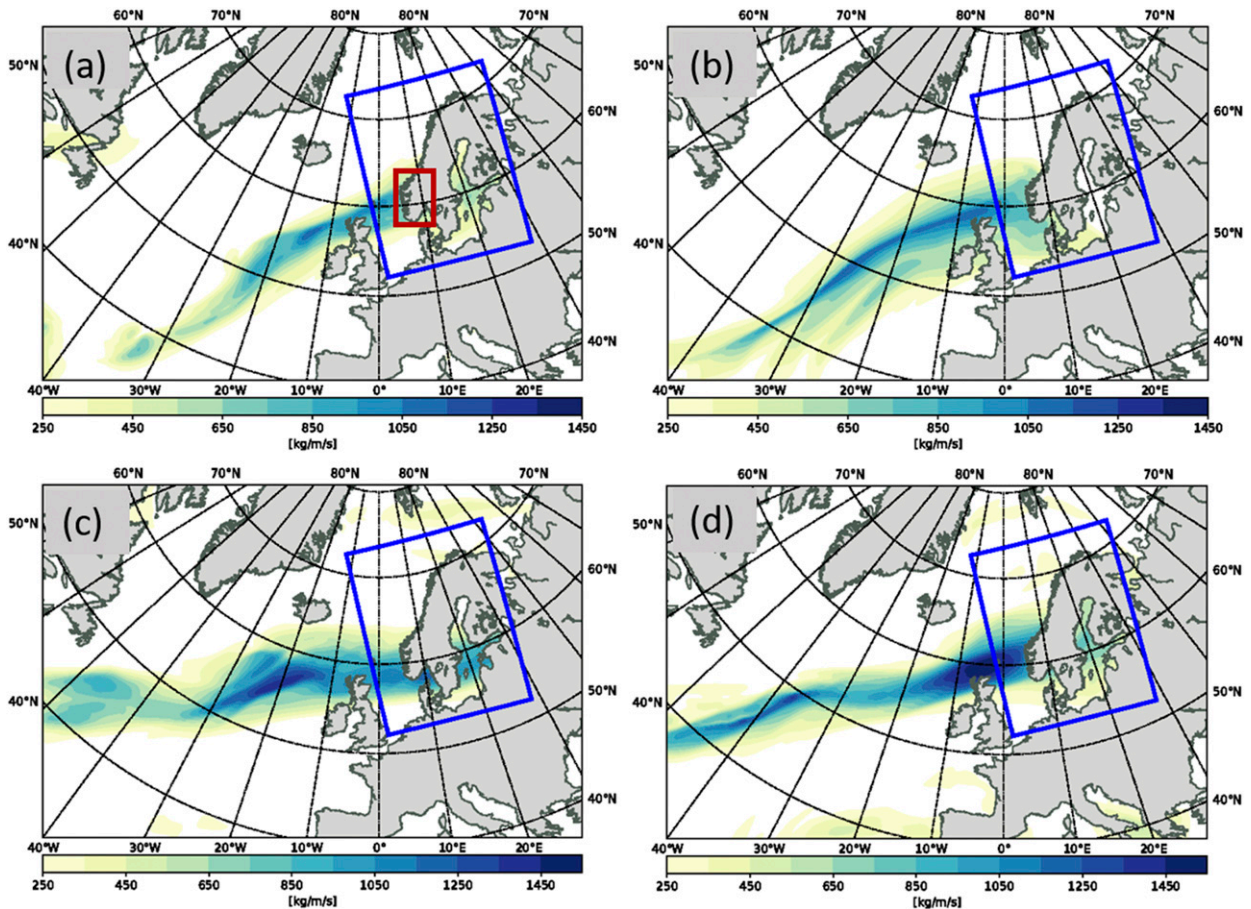Müller et al. (2017) compared precipitation intensity from AROME-MetCoOp, ECMWF IFS, and observed

FIG. 4. The figure illustrates the EC-Earth model integrated water vapor transport (IVT) for the selected atmospheric river events: (a) pr-1, (b) pr-2, (c) fu-1, and (d) fu-2. The blue box indicates the AROME-MetCoOp domain, whereas the red box in (a) indicates the domain used to present the results of this study and includes western Norway.

station data for an atmospheric river event in October 2014 and in addition, by using a spatial verification technique over a longer time span, they showed that ECMWF IFS predicts large-scale patterns reasonably well. There is, however, a significant advancement using the high-resolution system, which could mainly be explained by better representation of orographic precipitation forcing. In Fig. 5, the 24-h accumulated precipitation during the 2005 atmospheric river event is presented, and shows that the AROME-MetCoOp model, forced with ERA-Interim, is able to reproduce the precipitation pattern compared to the gridded observations (seNorge; Lussana et al. 2018). The seNorge data are, however, too smooth, since they use a spatial interpolation scheme in an area of complex topography in order to grid the relative sparse observational network. From the above evaluation, we find that precipitation is reasonably well represented in this study, even though precipitation amounts from AROME-MetCoOp forced with ERA-Interim are low compared to the

gridded observations, and therefore should be considered as lower limits.

The AROME-MetCoOp gridded temperature and precipitation data were prepared for the hydrological model by first aggregating the gridded data to daily time resolution, and thereafter calculating the average for each catchment. All four atmospheric river events, which each consist of 10 realizations with a duration of 6 days, were used as forcing for the hydrological model.

d. Hydrological model

The conceptual precipitation–runoff model HBV (Hydrologiska Byråns Vattenbalansavdelning) (Bergström 1976) as described in Sælthun (1996) and Beldring (2008) and implemented in the operational Norwegian flood-forecasting service, was used to estimate the streamflow. HBV has model components describing snow, soil moisture, and groundwater processes. The model is forced with daily catchment average temperature and precipitation. Within the HBV model, each catchment is
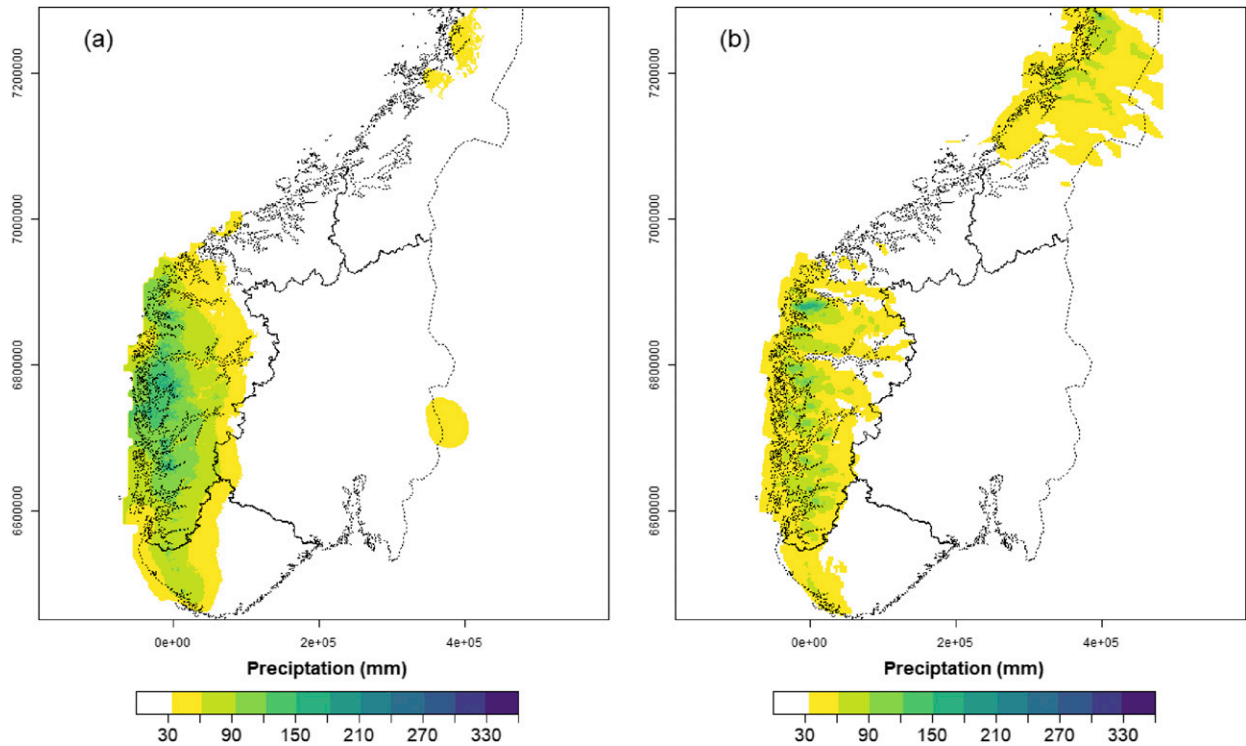
FIG. 5. Precipitation accumulated over 24 h for 0600 UTC 14 Sep 2005 from (a) seNorge v2.0, interpolated observations and (b) AROME-MetCoOp, run with ERA-Interim as boundary conditions. The geo reference in seNorge $1 \times 1 \, km^2$ grid is WGS84, UTM33 (m).

subdivided into 10 elevation zones, each elevation is chosen to yield 10 equal areas, and thereby account for vertical temperature and precipitation gradients.

All hydrological model parameters are optimized using seNorge observational precipitation and temperature data (Tveito 2002; Tveito et al. 2005; www.seNorge.no) as forcing, and streamflow observations from the hydrological database at NVE (https://www.nve.no/hydrology/) as the reference. The seNorge dataset is observational in situ data interpolated to a $1 \times 1 \, km^2$ grid available from 1 January 1957 until today. The Nash–Sutcliffe efficiency (Nash and Sutcliffe 1970) and volume bias are used as calibration and validation metrics. The Nash–Sutcliffe efficiency (positively oriented with an optimal value of 1) averaged for all catchments is for the calibration period 0.74 with zero volume bias, and 0.71 with 2.2% volume bias for the validation period. The calibration is done for all year daily data for the period 1996–2012, whereas the validation is conducted from 1980 to 1995. This study used the same setup and parameters as the operational flood-forecasting model.

Catchments in the western region, as defined in Vormoor et al. (2016), were used to evaluate the hydrological impact of the atmospheric river events. We chose to include catchments situated outside the event selection area (as in Fig. 3) to give a better description of

the spatial impact of the events. The 37 catchments are part of the operational flood-forecasting service for Norway and most of them are located in unregulated or weakly regulated rivers. Figure 3 shows the location and area of these catchments, defined by the natural drainage area for a measuring point in the river (the gauging station). The upstream areas vary in size and elevation, and for western Norway, the catchments are steep and relatively small (from 3 to 2400 km^2). Both elevation gradient and size can affect the timing and magnitude of a flood peaks. Most of the western catchments will reach the flood peak within one day of extreme precipitation. When the response time in a catchment is smaller than the model time steps, the model underestimates the flood peaks. However, current practice shows that we still get useful information on daily average flood sizes. In addition, we are evaluating the impact of atmospheric river events, lasting 24–72 h, as opposed to convective precipitation events where the subdaily time step is more critical.

In Norway, flood warnings are issued when floods exceed three predefined thresholds for daily average floods. Since there can be a discrepancy between the hydrological flood estimate and the observed values during floods, operational warning threshold are based on hydrological simulations using 60 years of seNorge

TABLE 1. A summary of precipitation and temperature for the selected historical years. The anomaly refers to the normal (reference period is 1961–90). The values represent statistics for the whole year (annual), season (autumn), and month (October) (https://www.yr.no/place/Norway/Sogn_og_Fjordane/Aurland/Fl%C3%A5m~124317/climate.html?spr=eng).

Ic	Year	Annual			Autumn			October		
		P	T (°C)	ΔT (°C)	P	T (°C)	ΔT (°C)	P	T (°C)	ΔT (°C)
A	2014	102.1%	5.3	2.5	87.7%	6.0	2.6	142%	6.2	2.3
B	1997	110.9%	3.4	0.8	96%	2.9	−0.3	115.8%	1.3	−2.3
C	1983	141.8%	2.9	0.3	161%	3.2	0.0	226.3%	3.1	−0.5
D	1960	65.5%	2.9	0.3	37.3%	3.3	0.1	22.7%	1.9	−1.6

observations as input. In this study, we used the operational warning levels as flood references, for example, the mean annual flood (RM), the 5-yr return level (R5), and the 50-yr return level (R50). To enable an easy comparison, the same flood thresholds were used for the present and the future events. Associated warning colors are yellow, orange and red; green is used to indicate streamflow below RM. We also extracted the maximum flood (Rmax) from these simulations and used Rmax as a reference maximum flood.

e. Hydrological initial conditions and evaluation

In operational flood forecasting, the hydrological initial states are established by either assimilating the observed states, or by running the hydrological model with meteorological observations. The hydrological initial conditions describe the state of the water storages in catchments and are important for the catchment response to rain and snowmelt. For events of short duration, here less than 6 days, the hydrological initial conditions will affect simulated streamflow, and in this study, we wanted to investigate the impacts of this effect.

The HBV model has storages for soil moisture, groundwater, and snow. We selected a set of four different characteristic initial conditions that we combined with all atmospheric river events. The hydrological initial conditions were selected to represent characteristic combinations of snow and soil moisture storages, and they were established by running the hydrological model with selected years of seNorge observational data. We selected years that represent contrasting combinations of temperature (low, high) and precipitation (dry, wet). The selection basis was the October weather statistics for western Norway. Table 1 presents the October average temperature and precipitation for the four selected year (2014, 1992, 1983, and 1960), as well as the deviation from the normal period. We hereafter label the hydrological initial conditions as A, B, C, and D, respectively. Figure 6 illustrates the state of snow storage and soil moisture deficit for the four initial conditions on 24 October, calculated by a distributed HBV model (seNorge.no). The internal states from the

distributed model can differ, but only slightly, from the internal states of the catchment models. From Fig. 6 we see that hydrological initial condition B and D are relatively dry, whereas A and C are wet. The snow storage depends on past precipitation and temperature. There is little snow present in A and D, whereas larger areas are snow covered for both B and C. In the following the initial conditions will be described as SNOW or BARE (no snow), and the soil moisture deficit as WET or DRY. The four initial conditions can be described as A: BARE-WET, B: SNOW-DRY, C: SNOW-WET, and D: BARE-DRY.

Different sets of hydrological initial conditions allowed us to evaluate how future floods are affected not merely by the dynamical forcing, as precipitation and temperature, but also by the initial states, like soil moisture and snow, in the hydrological modeling. We used the spread in the flood realizations to evaluate the contribution caused by hydrological initial conditions and ensemble realizations. We recall that for each catchment and event, 40 different flood realizations were created by using input data from 10 realizations (the perturbations in the EC-Earth model) and four different hydrological initial conditions. We used relative mean absolute deviation (RMAD) around the mean of the flood realizations as a dimensionless measure of ensemble spread.

The RMAD_e caused by the ensemble realizations (i.e., the meteorological forcing), was calculated as follows. First, the mean of the floods $\overline{q}_{\mathrm{ic}}$ simulated by the 10 ensemble realization, was calculated for each hydrological initial condition separately and used as the central tendencies. Thereafter, the relative deviation around each $\overline{q}_{\mathrm{ic}}$ caused by the ensemble realizations was calculated. Finally, the average of the four RMAD by the four hydrological initial conditions was calculated:

$$\mathrm{RMAD}_e = \frac{1}{4}\sum_{\mathrm{ic}=1}^{4}\frac{1}{10}\sum_{e=1}^{10}\left|\frac{q_{\mathrm{ic},e} - \overline{q}_{\mathrm{ic}}}{\overline{q}_{\mathrm{ic}}}\right|. \quad (1)$$

Similarly, the $\mathrm{RMAD}_{\mathrm{ic}}$ for the hydrological initial conditions were assessed by first calculating the deviation
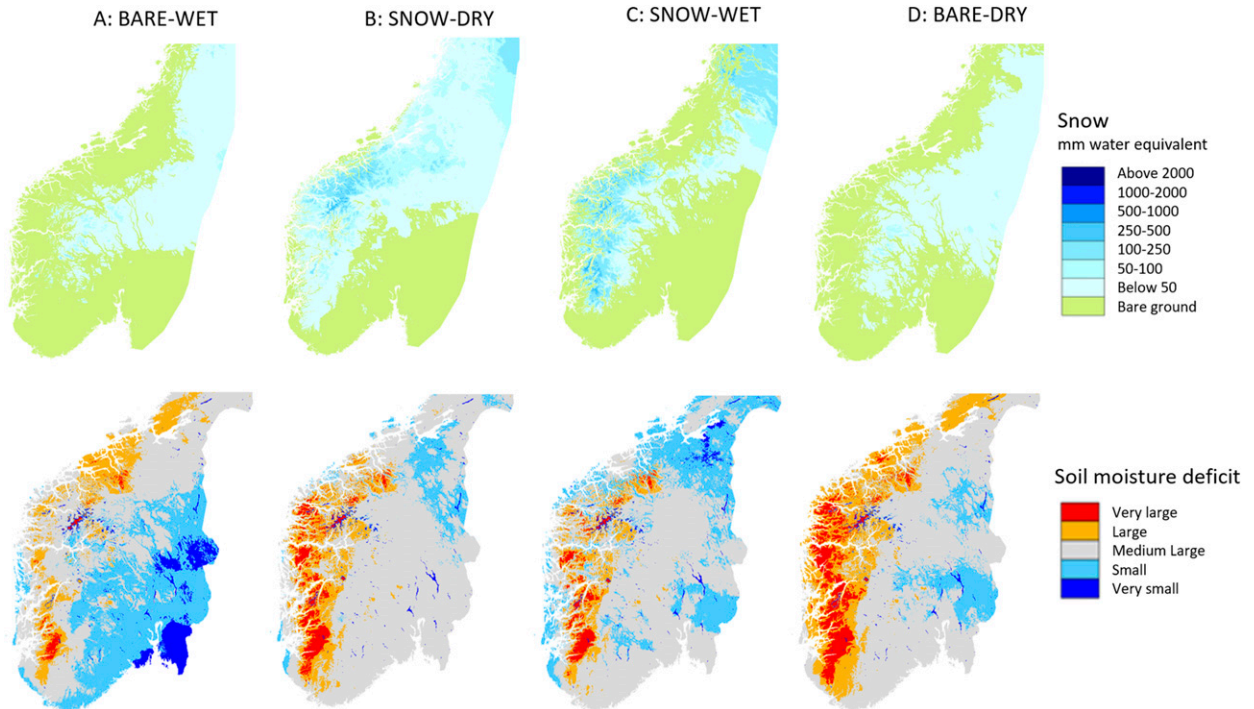
FIG. 6. (top) Snow storage and (bottom) soil moisture deficit, illustrating the four different hydrological initial conditions used in the HBV model. For snow (mm), the blue colors indicate snow, and green bare ground. For soil moisture deficit, the red color indicates very dry conditions, whereas blue indicates wet. The soil moisture deficit indicates to which percentile, defined by a reference period (1980–2010), the daily value categorizes. The 5th, 25th, 50th, 75th, and 95th percentiles of the reference period define the categories from "very small/wet" to "very large/dry."

around each ensemble realizations due to the hydrological initial conditions, using the mean of the ensemble realizations $\overline{q}_e$ as the central tendency:

$$\text{RMAD}_{ic} = \frac{1}{10} \sum_{e=1}^{10} \frac{1}{4} \sum_{ic=1}^{4} \left| \frac{q_{ic,e} - \overline{q}_e}{\overline{q}_e} \right|. \qquad (2)$$

We calculated the RMAD only at the time of the flood peak for each event. By comparing RMAD_e to RMAD_{ic} in a scatterplot, we can assess the importance of the ensemble realizations and the hydrological initial conditions to the spread in simulated flood sizes. Both RMAD_e and RMAD_{ic} will have a value between 0 and 1.

3. Results and discussion

a. The precipitation events

Figure 7 illustrates the spatial distribution of 132 h accumulated precipitation during the four atmospheric river events simulated with AROME-MetCoOp and averaged over the 10 realizations. The future (fu) events fu-1 (Fig. 7c) and fu-2 (Fig. 7d) have more precipitation, and especially coastal precipitation is higher compared to present (pr) events pr-1 (Fig. 7a) and pr-2 (Fig. 7b).

The IVT of both future events are higher (Figs. 4c,d), and are located more to the north, compared to the present events. The higher moisture content in the future events means that precipitation will fall out at lower elevation. (i.e., closer to the coast). This finding is supported by Sandvik et al. (2018) conducting a study for the Norwegian west coast. They find that an increase in temperature (as in a future climate) causes a larger increase in near-coastal precipitation compared to more inland precipitation.

Pr-1 has overall less precipitation than the other events. Whereas pr-2, which has below zero temperatures for larger parts of the domain, has some precipitation peaks, located at the highest elevations, and over glaciered areas. The peaks in pr-2 seem to be induced by the downscaling, but do not affect flood magnitudes, since the temperatures are well below zero.

b. Flood evaluation

1) FLOOD WARNING LEVELS

For all catchments and realizations, we determined the floods exceedance of operational flood warning thresholds. Figure 8 gives an overview of catchments
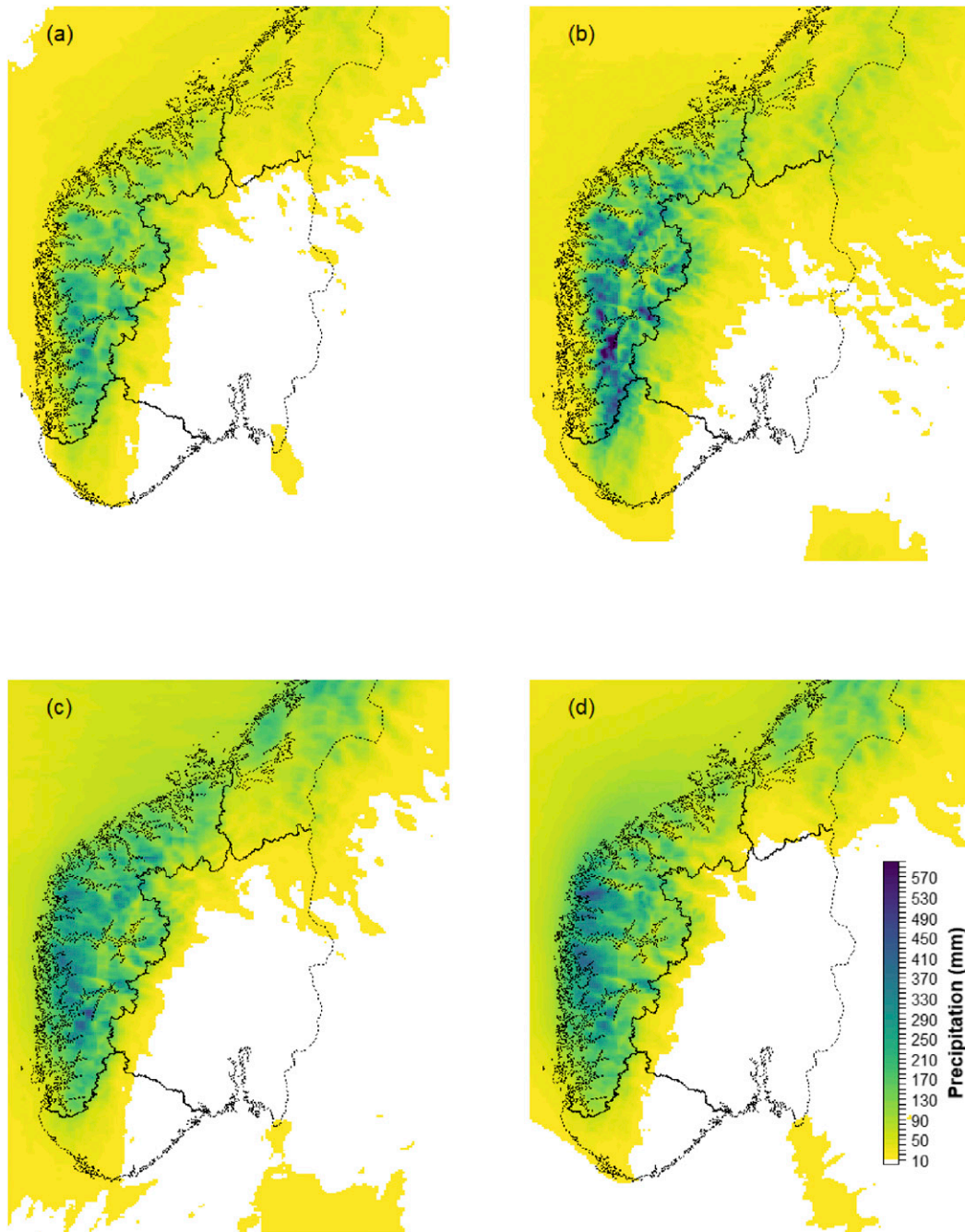
FIG. 7. Accumulated precipitation (132 h) for present events (a) pr-1 and (b) pr-2 and future events (c) fu-1 and (d) fu-2. All values are the average of 10 realizations of AROME-MetCoOp precipitation.

with no floods (green) and catchments where at least one flood realization reached the warning levels of mean annual flood (yellow), 5-yr flood (orange), and 50-yr flood (red), which are the official warning levels in Norway. In each colored cell, the number indicates the percentage of realizations (10 members in each cell) that exceeded the red level. The columns in Fig. 8 represent both present and future events combined with the four different initial conditions, A–D (Table 1). Each row shows the results for one catchment. The last row, however, represents the percentage of R50 exceedances that includes all catchments and is therefore a summary of the combined effect of initial conditions and events on floods over the larger area. Figure 8 highlights that the

FIG. 8. An overview of warning levels for the combination of events and initial conditions (columns A–D) for all 37 catchments (rows). The colors indicate the flood warning level exceeded, while the numbers within the red cells indicate the percentage of ensemble members reaching a red warning level for that specific combination of event and initial condition. The total red warning levels reached for each catchment (% mbrs > R50), and the maximum flood level ($m^3 s^{-1}$; Qmax) estimated for any of the events is presented in columns. The gray colored cells indicate the highest Qmax value for each catchment comparing future and present events, whereas pink colored cells indicate the highest streamflow value comparing Qmax to Rmax ($m^3 s^{-1}$). The last row represents the percentage of R50 exceedances for all catchments and is therefore a summary of the combined effect of initial conditions and events on floods for the larger area.

red warning level is reached for more catchments in the future compared to the present events, from 23 to 11, respectively. Moreover, for the future events, a higher number of the realizations reached the highest warning level (% mbrs > R50), totally 18.9% in the future and

6.1% in the present climate (see % mbrs > R50 in columns 10 and 20 in Fig. 8). By dividing the total number of realizations from Fig. 8 by the number of catchments impacted summarized from Table 2, we find that on average there are 3.8 realizations per red warning in the

TABLE 2. Total number of catchments where streamflow exceeds red warning levels, indexed by initial conditions and events. Initial conditions (ic) are based the soil moisture and snow conditions from Fig. 7, which refers to Oct data for selected years (Table 1).

Ic event	A: BARE-WET	B: SNOW-DRY	C: SNOW-WET	D: BARE-DRY	Red/event
Pr-1	5	7	7	2	21
Pr-2	6	7	8	5	26
Fu-1	13	19	20	7	59
Fu-2	14	13	15	9	51
Red/ic	38	46	50	23	157

present climate, and 5.1 realizations per red warning in the future climate. Overall, the results show that more catchments and more realizations reached a red warning level in the future events.

The flood magnitude is important for the assessment of flood impact, since the magnitude directly relates to damage potential. To evaluate the possible maximum impact from the present and the future realizations, we select the highest flood value (Qmax; $m^3 s^{-1}$) for each catchment; hence, each Qmax was selected from two events and 40 realizations per event. Qmax representing the present and the future climate (Fig. 8) were compared with each other and to the reference maximum floods (Rmax). Note that Rmax is the highest daily flood value estimated running the hydrological model with 60 years of seNorge temperature and precipitation observational data and is not constrained to atmospheric river events. The evaluation shows that Qmax for the future events is higher than Qmax for the present events for 22 of 23 catchments that reached a red warning for the future events (gray or pink colored cells in the last column in Fig. 8). The future highest floods are larger than the reference floods (Rmax) for 14 of the same 23 catchments, whereas none of the present climate floods exceeds Rmax.

In summary, these results show that for the future atmospheric river events, more catchments will reach a red warning level during the same event. For these catchments, the daily flood peaks will be higher, and more realizations will reach a red warning level, indicating that extreme floods coinciding in multiple catchments are more likely in the future. It is important to note that the results are conservative and might underestimate the flood risk for two reasons: (i) we are using a moderate RCP4.5 scenario and (ii) the extreme precipitation of the events seems to be low compared to the gridded interpolated observations (Fig. 5).

2) HYDROLOGICAL INITIAL CONDITIONS

Figure 8 moreover holds information on the sensitivity of floods to initial conditions, expressed by the change in warning colors with the initial conditions A–D for several of the catchments. Table 2 summarizes the catchments from Fig. 8 exceeding a red level. Snow in

the catchments clearly contribute to increased floods, the total number of catchments exceeding red level for all events was 96 for SNOW (B and C) versus 61 for BARE (A and D). The difference between catchments exceeding the red level for SNOW-DRY (46) and SNOW-WET (50) is relatively small; illustrating that snow is the most important hydrological initial condition in this area. The soil moisture is more important when there is little or no snow available, for BARE-WET 38 catchments exceed the red warning level compared to BARE-DRY where 23 exceeded, which indicate an increase in number of exceedances of 65% when conditions are wet. By contrast, when snowpack is significant, there is an increase of only 11% under wet versus dry soil moisture conditions.

The initial conditions for a future scenario are more likely to be similar to A (BARE-WET), since climate projections indicate a warmer and wetter west coast climate (Baatsen et al. 2015; Hanssen-Bauer et al. 2017). However, variabilities in weather in the future should also be anticipated, and the exceptional October 2018 flood event in western Norway exemplified (see section 1) the importance of the variability in temperature and precipitation during autumn. The presence of snow that is available for melt followed by a warm and moist atmospheric river event (extreme precipitation) has historically shown to cause some of the most severe flood impacts (Roald 2008). Figure 8, thus, illustrates that accounting for different hydrological initial conditions in the climate–hydrological modeling chain adds value to the flood impact evaluation. The antecedent conditions and the memory of the catchment, for example, groundwater, soil moisture, water levels in lakes, and snow, are all important for the catchment response to extreme precipitation.

3) SPATIAL FLOOD IMPACT

Historical atmospheric river events clearly show that the spatial impact and severity of the events varies. Which and to what extent catchments are affected by an atmospheric river depends on several factors: the atmospheric conditions (e.g., the placements of pressure systems), the extent and duration of the atmospheric river, the moisture content, the temperature, and the intensity and duration of precipitation during the event.
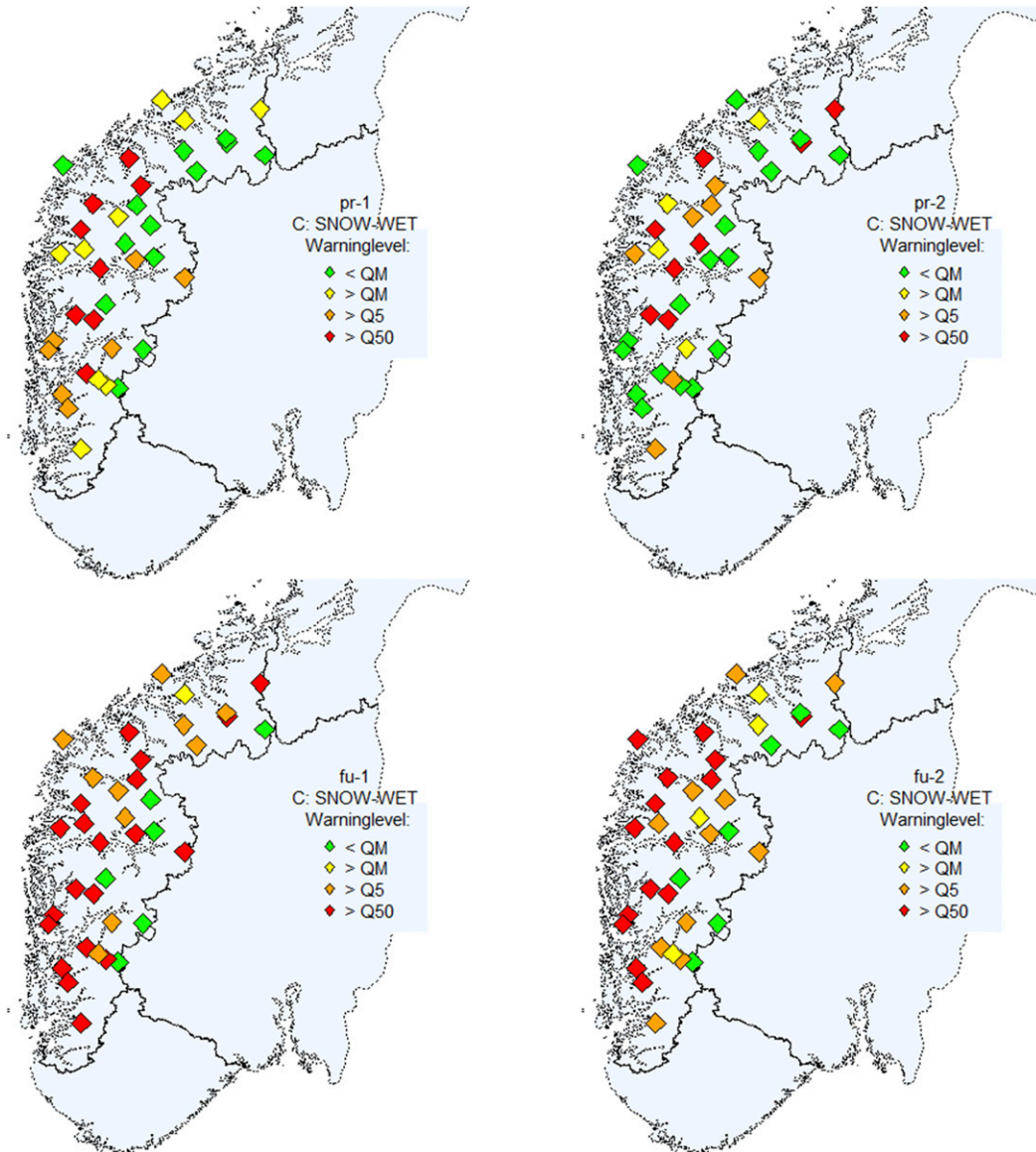
FIG. 9. The spatial distribution of the warning levels for catchments in western Norway, SNOW-WET (C) used to establish initial conditions. The highest warning level reached for each catchment is presented for all events: (top) pr-1 and pr-2 (present climate) and (bottom) fu-1 and fu-2 (future climate). Yellow (RM), orange (R5), and red (R50) diamonds define floods exceeding the warning thresholds, whereas green diamonds indicate no floods.

We used the maximum flood level reached at each catchment to visualize the spatial impact of the four atmospheric river events, presented by separate maps in Fig. 9. SNOW-WET (C) was used as hydrological initial condition for all events, since it was the hydrological initial condition that resulted in the highest number of catchments exceeding the red flood level in both present and future climate (Table 2).

Figure 9 shows that the future events affect more catchments closer to the coast than the present events. This seems to be in line with Sandvik et al. (2018). They

used an idealized temperature perturbation to study the effect of temperature increase on precipitation and found that near-coastal, high-elevation areas experienced the highest increase in extreme precipitation. Apart from higher future floods for the coastal catchments, there are no other clear patterns to be seen in Fig. 9. Not all catchments were affected by all events, mainly because each landfall is unique, and some areas are missed by the most intense precipitation. In a few catchments, however, a temperature below freezing at higher elevations cause precipitation to classify as snow

in parts of catchment, and for these catchments high precipitation does not generate floods. Event pr-2 is relatively cold, which resulted in fewer floods even if the precipitation was high (Fig. 4b).

We find that Fig. 9 demonstrates an advantage of the event-based approach by providing a plausible image of the possible impact of single events, using a well-known modeling chain and flood exceedance levels. This way, it is easier to present how future atmospheric river events, that contain more precipitation due to a warmer climate, have a higher impact over a larger spatial area with severe floods occurring in multiple catchments within a short time span.

c. Sensitivity to ensemble spread and hydrological initial conditions

The spatial differences in precipitation combined with the hydrological initial conditions will determine how floods evolve and unfold in different catchments. To visualize the different flood impacts and the range of possible outcomes, detailed results for six catchments are presented in Fig. 10, with catchment characteristics shown in Table 3. Each boxplot in Fig. 10 represents 40 realizations and reveals the range in streamflow estimates due to the combination of meteorological ensemble realizations and the hydrological initial conditions.

Øye and Lovatn are located north in the study domain and outside the event selection area. Despite a spatial proximity (35-km distance, but in different fjords), they reveal different streamflow response to the same atmospheric river events. The spread in the streamflow response to meteorological forcing and hydrological initial conditions are larger for Øye than Lovatn. Nautsundvatn, Hovefoss, and Røykenes are all near-coastal catchments with similarities in catchment characteristics. The high future floods are representative for the increased near-coastal precipitation seen in fu-1 and fu-2 (Fig. 4). The three catchments all show a similar response to the precipitation, with respect to both magnitudes and timing. Røykenes and Bulken, on the other hand, illustrate contrasting flood responses. Røykenes is an example of a small and steep catchment with a quick streamflow response to precipitation, whereas for Bulken, with a larger catchment area, streamflow rises slower and the high streamflow lasts longer. Bulken is positioned central within the event selection area and is affected by high floods in both the present and future simulations.

The large spread in the flood estimates (boxplots in Fig. 10) indicates sensitivity to the hydrological initial conditions and/or the temperature and precipitation forcing. The large spread demonstrates that an ensemble of realizations is important to capture the highest floods that pose the highest damage potential. The spread can be attributed both to the ensemble realization and to the hydrological initial conditions. In Fig. 11, using RMAD as a measure of spread [see Eqs. (1) and (2)], we find that for most events and catchments, the ensemble realizations contribute most to the spread, however, for some events and catchments, the hydrological initial conditions contribute more. Figure 11 does not reveal any clear pattern that would explain whether spread caused by ensembles realizations or hydrological initial conditions were more important for any catchments, however, for all catchments in pr-1 and fu-2 the ensemble spread has the highest contribution to the spread in the flood estimates. For the catchments and events in Fig. 11, we find that ensemble realizations can change the streamflow estimates by over 60% (Øye, pr-1), whereas the initial conditions can alter the estimates by nearly 30% (Nautsundvatn, pr-1). Mostly the contribution to spread caused by both hydrological initial conditions and ensemble realizations are between 10% and 20%. An evaluation that included all catchments gave similar results.

d. Final remarks on the event-based approach

In this study, we used a small sample size, which in a traditional setup would mean that we could not draw any conclusions to whether our results are due to natural variability or from climate change. We present 40 EC-Earth realizations per catchment, whereof 20 are set in a future and 20 in a present climate. All realizations are from one climate model, compared to multimodel ensembles used in most climate projection studies (e.g., Sillmann et al. 2013), and our results represent only one emission scenario (RCP4.5). Nevertheless, we believe that the event-based approach provides supplementary information about future flood risk in western Norway. First, our results are in accordance with previous studies of climate change in this region. They show increased precipitation in western Norway independent of model or emission scenario (e.g., Hanssen-Bauer et al. 2017), and our events are hence representative for these scenarios. Moreover, Whan et al. (2020) show that the extreme precipitation and atmospheric river statistics in the present climate EC-Earth simulations is similar to the observed relationship (ERA-Interim), and that in a future climate the frequency of atmospheric rivers and the intensity of each event increases. We further know that the high-resolution EC-Earth model is suitable to model the precipitation onto the topography of the west coast of Norway, and we can assume that the events are plausible under both the present and the future climate. In addition, we used the operational AROME-MetCoOp
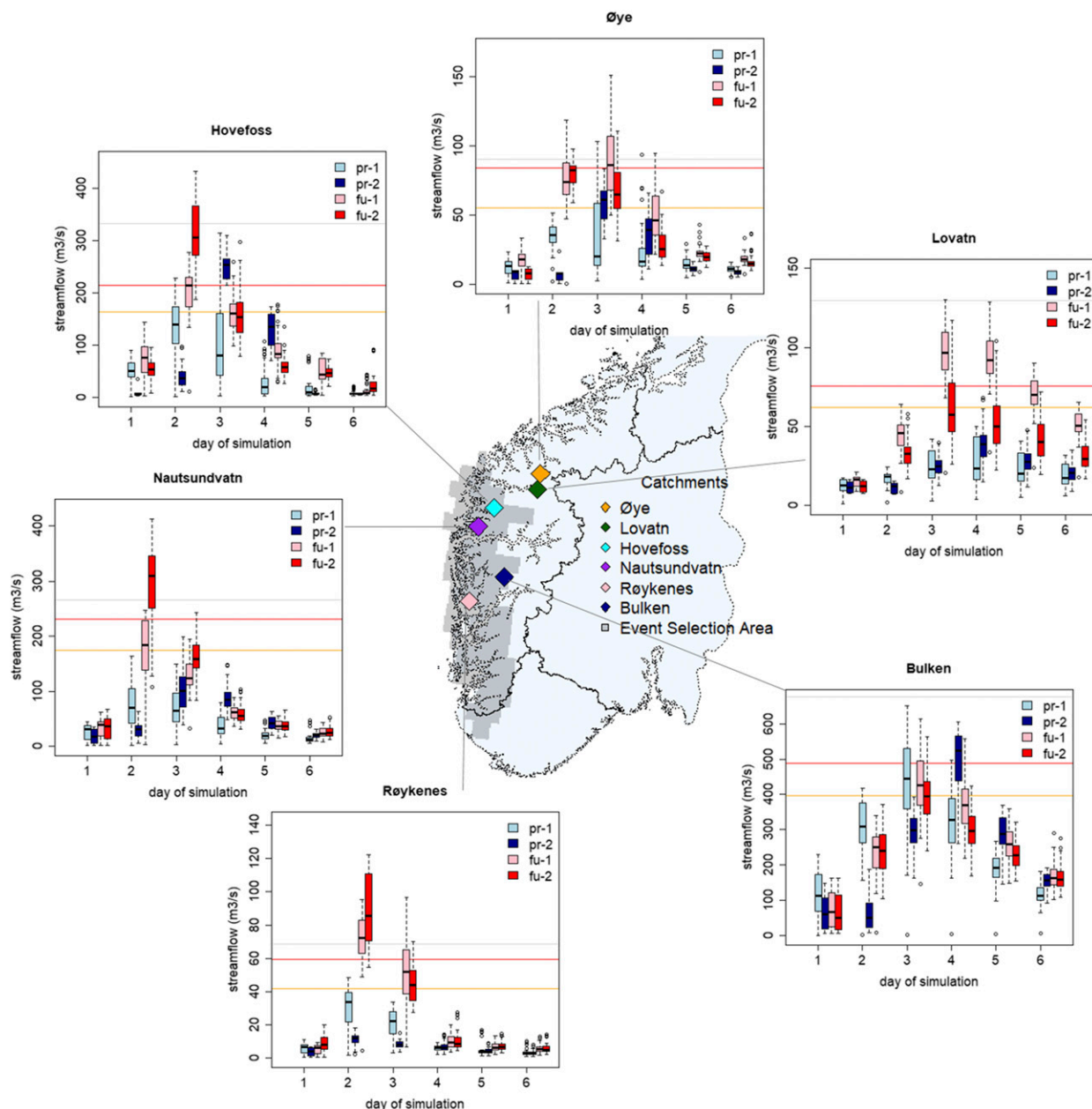
FIG. 10. Hydrographs of boxplots showing the 4 × 10 estimated floods for six selected catchments. Present events are colored blue: pr-1 is light blue, pr-2 is blue, and future events are colored green: fu-1 is light-green (pink), and fu-2 is green (red). The horizontal orange and red lines are the thresholds for 5- and 50-yr floods, while the gray line is the reference maximum floods (Rmax), which is calculated from 60 years of seNorge data for respective catchments; the y axis is streamflow and x axis is days of the simulated event. Each box contains 40 values, the box itself defines the 25th–75th percentile, and the whiskers max 1.5 times the box extension with any values outsides indicated as circular outliers.

weather prediction model, which improves the representation of extreme precipitation events (Müller et al. 2017), and the operational HBV models to finally estimate the floods. We kept the physical consistency of the variables throughout the modeling chain and could hence provide physically plausible flood events. The similarities to the operational modeling chain, makes

the results easily accessible to both flood management and scientist.

4. Summary and conclusions

We compared possible flood events in a future warmer climate to those in a present climate by analyzing four

TABLE 3. Catchment characteristics for catchments in the case study. Area is the catchment area upstream the gauging station, annual precip is the annual catchment average precipitation, lake fraction is the lake covered area in percent of total area, steepness is (max elev − min elev)/area, min elev is minimum catchment elevation, and max elev is maximum catchment elevation.

Catchment	Area (km^2)	Annual precip (mm)	Lake fraction (%)	Steepness $(m\,km^{-2})$	Min elev (m MSL)	Max elev (m MSL)
Øye	138	976	0.26	12.25	147	1848
Lovatn	234	2041	4.5	8.59	52	2071
Hovefoss	234	2796	0.45	6.18	20	1469
Nautsundvatn	219	3043	2.16	3.92	45	904
Bulken	1092	2037	0.87	1.42	47	1602
Røykenes	50	3176	2.24	18.12	53	960

representative extreme precipitation events associated with atmospheric rivers reaching the west coast of Norway. In addition, we introduced four different hydrological initial conditions, established using historical data, to evaluate the importance of antecedent weather on floods, and thereby uncertainties introduced by the hydrological initial conditions. We followed an event-based approach that particularly facilitates the use of a modeling chain similar to the operational weather- and flood-forecasting chain. This approach enabled us to easier interpret the possible impact of such events and makes the results accessible to both a scientific and a management audience.

This study shows the following:

- The future atmospheric river events affect larger areas compared to the present events. We found that the future events caused floods in more catchments, and the floods were at a higher magnitude.
- As each event is unique, the landfall of the atmospheric rivers is difficult to determine beforehand. Hence, applying hydrological modeling to several catchments within a larger area was important to capture the total spatial flood impact of each event.
- Hydrological initial conditions, for example, soil saturation and snow storage, affected the flood magnitude for most of the catchments and for all events. Available snow increased the number of catchments in flood due to the added contribution from snowmelt, whereas dry and snow free conditions reduced the number of catchments in flood. Snow storage was the most important initial condition, showing that an atmospheric river event following a period with snow accumulation has the highest damage potential.
- The ensemble realizations, representing different precipitation intensities, were the major contributor to spread in the flood estimates for most catchments, however, for one quarter of catchments and events, the hydrological initial conditions exhibited an important contribution to the spread.

We acknowledge that this event-based approach, which contains results from a few plausible events, based on only one climate model and only one emission scenario, will not provide enough data to provide any probabilities for future floods. We do, however, provide high-resolution modeling, well adopted to describe atmospheric rivers in both the present and the future climate. Further event-based studies could include events simulated in different emission scenarios like the RCP8.5, which projects even more extreme precipitation for western Norway.

The benefit of the event-based approach is that the events are easier to visualize and to communicate, than for example multimodel ensemble probabilities. The event-based approach is therefore a useful supplementary to raise the awareness of possible future impact, caused by physically plausible extreme events. The chosen approach
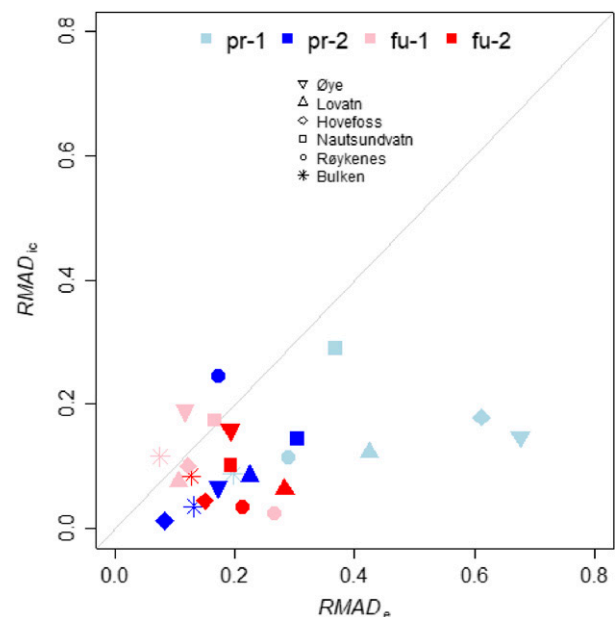

FIG. 11. The same catchments as in Fig. 10, but here the contributions to spread seen in the boxplots are separated to that caused by the ensemble realizations representing the meteorological forcing (e) and the hydrological initial conditions (ic). Relative mean absolute deviation caused by the ensemble realizations ($RMAD_e$) is on the x axis, and the relative mean absolute deviation caused by the hydrological initial conditions ($RMAD_{ic}$) is on the y axis.

operates very closely to current operational procedures, using a strategic modeling chain ranging from GCMs over RCMs to hydrological models; this makes it accessible to both the scientific community and a management audience. Floods, which are often accompanied by landslides, are demanding situations for rescue and emergency preparedness and cause high economic and social losses in affected areas. By providing information that implies that future events most likely will affect more catchments, and hence involve more municipalities simultaneously, such information can reveal some future challenges for, for example, municipalities and railway and road authorities. These future challenges underline the need for joint preparedness across, for example, community boarders for exposed and vulnerable areas.

Data availability statement: Data are available upon reasonable request from NVE (HBV), MetNorway (AROME-MetCoOp), and KNMI (EC-Earth). SeNorge data are available from the free meteorological data portal (https://www.met.no/en/free-meteorological-data/Download-services), and discharge measurements are available from the hydrological database at NVE (https://www.nve.no/hydrology/).

REFERENCES

Azad, R., and A. Sorteberg, 2017: Extreme daily precipitation in coastal western Norway and the link to atmospheric rivers. *J. Geophys. Res. Atmos.*, **122**, 2080–2095, https://doi.org/10.1002/2016JD025615.

Baatsen, M., R. J. Haarsma, A. J. Van Delden, and H. de Vries, 2015: Sever Autumn storms in future Western Europe with a warmer Atlantic Ocean. *Climate Dyn.*, **45**, 949–964, https://doi.org/10.1007/s00382-014-2329-8.

Beldring, S., 2008: Distributed element water balance model system. NVE Rep. 4, 42 pp., http://publikasjoner.nve.no/report/2008/report2008_04.pdf.

Benedict, I., K. Ødemark, T. Nipen, and R. Moore, 2019: Large-scale flow patterns associated with extreme precipitation and atmospheric rivers over Norway. *Mon. Wea. Rev.*, **147**, 1415–1428, https://doi.org/10.1175/MWR-D-18-0362.1.

Berghuijs, W. R., S. Harrigan, P. Molnar, L. J. Slater, and J. W. Kirchner, 2019: The relative importance of different flood-generating mechanisms across Europe. *Water Resour. Res.*, **55**, 4582–4593, https://doi.org/10.1029/2019WR024841.

Bergström, S., 1976: Development and application of a conceptual runoff model for Scandinavian catchments. SMHI RHO Rep. 7, 134 pp.

Bintanja, R., C. Severijns, R. Haarsma, and W. Hazeleger, 2014: The future of Antarctica's surface winds simulated by a high-resolution global climate model: 1. Model description and validation. *J. Geophys. Res. Atmos.*, **119**, 7136–7159, https://doi.org/10.1002/2013JD020847.

Caroletti, G. N., and I. Barstad, 2010: An assessment of future extreme precipitation in western Norway using a linear model. *Hydrol. Earth Syst. Sci.*, **14**, 2329–2341, https://doi.org/10.5194/hess-14-2329-2010.

Dee, D. P., and Coauthors, 2011: The ERA-Interim reanalysis: Configuration and performance of the data assimilation system. *Quart. J. Roy. Meteor. Soc.*, **137**, 553–597, https://doi.org/10.1002/qj.828.

Dettinger, M., 2011: Climate change, atmospheric rivers, and floods in California – A multimodel analysis of storm frequency and magnitude changes. *J. Amer. Water Resour. Assoc.*, **47**, 514–523, https://doi.org/10.1111/j.1752-1688.2011.00546.x.

Espinoza, V., D. E. Waliser, B. Guan, D. A. Lavers, and F. M. Ralph, 2018: Global analysis of climate change projection effects on atmospheric rivers. *Geophys. Res. Lett.*, **45**, 4299–4308, https://doi.org/10.1029/2017GL076968.

Haarsma, R. J., W. Hazeleger, C. Severijns, H. Vries, A. Sterl, R. Bintanja, G. J. Oldenborgh, and H. W. Brink, 2013: More hurricanes to hit Western Europe due to global warming. *Geophys. Res. Lett.*, **40**, 1783–1788, https://doi.org/10.1002/grl.50360.

Hanssen-Bauer, I., and Coauthors, 2017: Climate in Norway 2100 - A knowledge base for climate adaption. NCCS Rep. 1/2017, 48 pp.

Hazeleger, W., and Coauthors, 2010: EC-Earth: A seamless earth-system prediction approach in action. *Bull. Amer. Meteor. Soc.*, **91**, 1357–1364, https://doi.org/10.1175/2010BAMS2877.1.

——, B. J. J. M. van den Hurk, E. Min, G. J. van Oldenborgh, A. C. Petersen, D. A. Stainforth, E. Vasileiadou, and L. A. Smith, 2015: Tales of future weather. *Nat. Climate Change*, **5**, 107–113, https://doi.org/10.1038/nclimate2450.

Howarth, C., D. Viner, S. Dessai, C. Rapley, and A. Jones, 2017: Enhancing the contribution and role of practitioner knowledge in the Intergovernmental Panel on Climate Change (IPCC) Working Group (WG) II process: Insights from UK workshops. *Climate Serv.*, **5**, 3–10, https://doi.org/10.1016/j.cliser.2017.04.003.

Iden, K., K. Isaksen, S. Kristiansen, and H. Szewczyk-Bartnicka, 2005: Weather in Norway—Climatological monthly overview for September 2005 (in Norwegian). Meteorological Institute, Oslo, Norway, 18 pp., https://www.met.no/publikasjoner/met-info/met-info-2005.

IPCC, 2010: IPCC Expert Meeting on Assessing and Combining Multi Model Climate Projections: Meeting Report. T. Stocker et al., Eds., IPCC, 127 pp., https://www.ipcc.ch/site/assets/uploads/2018/05/expert-meeting-assessing-multi-model-projections-2010-01.pdf.

Kobierska, F., K. Engeland, and T. Thorarinsdottir, 2018: Evaluation of design flood estimates – A case study for Norway. *Hydrol. Res.*, **49**, 450–465, https://doi.org/10.2166/nh.2017.068.

Langsholt, E., L. A. Roald, E. Holmqvist, and A. Fleig, 2015: Flommen på Vestlandet oktober 2014 (in Norwegian). Norwegian Water Resources and Energy Directorate, Rep. 112015, 69 pp., http://publikasjoner.nve.no/rapport/2015/rapport2015_11.pdf.

Lavers, D. A., and G. Villarini, 2013: The nexus between atmospheric rivers and extreme precipitation across Europe. *Geophys. Res. Lett.*, **40**, 3259–3264, https://doi.org/10.1002/grl.50636.

——, and ——, 2015: The contribution of atmospheric rivers to precipitation in Europe and the United States. *J. Hydrol.*, **522**, 382–390, https://doi.org/10.1016/j.jhydrol.2014.12.010.

Lawrence, D., 2016: Klimaendringer og framtidige flommer i Norge (in Norwegian). Norwegian Water Resources and Energy Directorate Rep. 81-2016, 66 pp., http://publikasjoner.nve.no/rapport/2016/rapport2016_81.pdf.

——, and H. Hisdal, 2011: Hydrological projections for floods in Norway under a future climate. Norwegian Water Resources and Energy Directorate Rep. 5-2011, 47 pp., http://publikasjoner.nve.no/report/2011/report2011_05.pdf.

Lussana, C., T. Saloranta, T. Skaugen, J. Magnusson, O. E. Tveito, and J. Andersen, 2018: seNorge2 daily precipitation, an observational gridded dataset over Norway from 1957 to the present day. *Earth Syst. Sci. Data*, **10**, 235–249, https://doi.org/10.5194/essd-10-235-2018.

Maraun, D., 2016: Bias correcting climate change simulations - A critical review. *Curr. Climate Change Rep.*, **2**, 211–220, https://doi.org/10.1007/s40641-016-0050-x.

Müller, M., and Coauthors, 2017: AROME-MetCoOp: A Nordic convective-scale operational weather prediction model. *Wea. Forecasting*, **32**, 609–627, https://doi.org/10.1175/WAF-D-16-0099.1.

Nash, J. E., and J. V. Sutcliffe, 1970: River flow forecasting through conceptual models. Part I - A discussion of principles. *J. Hydrol.*, **10**, 282–290, https://doi.org/10.1016/0022-1694(70)90255-6.

Neiman, P. J., A. B. White, F. M. Ralph, D. J. Gottas, and S. I. Gutman, 2009: A water vapor flux tool for precipitation forecasting. *Water Manage.*, **162**, 83–94, https://doi.org/10.1680/WAMA.2009.162.2.83.

Olsson, J., and Coauthors, 2016: Hydrological climate change impact assessment at small and large scales: Key messages from recent progress in Sweden. *Climate*, **4**, 39, https://doi.org/10.3390/cli4030039.

Orvedal, K., and I. O. Peereboom, 2014: Flaumsonekart Delprosjekt Førde (in Norwegian). Norwegian Water Resources and Energy Directorate Rep. 61/2014, 42 pp., http://publikasjoner.nve.no/rapport/2014/rapport2014_61.pdf.

Persson, A., 2015: User guide to ECMWF forecast products. E. Andersson and I. Tsonevsky, Eds., ECMWF, 129 pp.

Porter, J. J., and S. Dessai, 2017: Mini-me: Why do climate scientists' misunderstand users and their needs? *Environ. Sci. Policy*, **77**, 9–14, https://doi.org/10.1016/j.envsci.2017.07.004.

Prein, A. F., and Coauthors, 2015: A review of regional convection-permitting climate modeling: Demonstrations, prospects, and challenges. *Rev. Geophys.*, **53**, 323–361, https://doi.org/10.1002/2014RG000475.

Ralph, F. M., and M. D. Dettinger, 2011: Storms, floods, and the science of atmospheric rivers. *Eos, Trans. Amer. Geophys. Union*, **92**, 265–266, https://doi.org/10.1029/2011EO320001.

——, and Coauthors, 2017: Atmospheric rivers emerge as a global science and applications focus. *Bull. Amer. Meteor. Soc.*, **98**, 1969–1973, https://doi.org/10.1175/BAMS-D-16-0262.1.

Roald, L. A., 2008: Rainfall floods and weather patterns. NVE Consultancy Rep. 14-2018, 44 pp., http://publikasjoner.nve.no/oppdragsrapportA/2008/oppdragsrapportA2008_14.pdf.

Sælthun, N. R., 1996: The Nordic HBV model. Description and documentation of the model version developed Tech. Rep. NVE-E-PUB-07/96, Norwegian Water Resources and Energy Administration Publ. 7, 27 pp.

Sandvik, M. I., A. Sorteberg, and R. Rasmussen, 2018: Sensitivity of historical orographically enhanced extreme precipitation events to idealized temperature perturbations. *Climate Dyn.*, **50**, 143–157, https://doi.org/10.1007/s00382-017-3593-1.

Sharma, A., C. Wasko, and D. P. Lettenmaier, 2018: If precipitation extremes are increasing, why aren't floods? *Water Resour. Res.*, **54**, 8545–8551, https://doi.org/10.1029/2018WR023749.

Shepherd, T. G., 2019: Storyline approach to the construction of regional climate change information. *Proc. Roy. Soc.*, **475A**, 20190013, https://doi.org/10.1098/rspa.2019.0013.

——, and Coauthors, 2018: Storylines: An alternative approach to representing uncertainty in physical aspects of climate change. *Climatic Change*, **151**, 555–571, https://doi.org/10.1007/s10584-018-2317-9.

Sillmann, J., V. V. Kharin, F. W. Zwiers, X. Zhang, and D. Bronaugh, 2013: Climate extremes indices in the CMIP5 multimodel ensemble: Part II. Future climate projections. *J. Geophys. Res. Atmos.*, **118**, 2473–2493, https://doi.org/10.1002/JGRD.50188.

Sorteberg, A., D. Lawrence, A. V. Dyrrdal, S. Mayer, and K. Engeland, Eds., 2018: Climate changes in short duration extreme precipitation and rapid onset flooding – Implications for design values. NCCS Rep 1/2018, 143 pp., https://cms.met.no/site/2/klimaservicesenteret/rapporter-og-publikasjoner/_attachment/13537?_ts=163df95ff7b.

Sterl, A., and Coauthors, 2008: When can we expect extremely high surface temperatures? *Geophys. Res. Lett.*, **35**, L14703, https://doi.org/10.1029/2008GL034071.

Stohl, A., Forster, C., and Sodemann, H., 2008: Remote sources of water vapor forming precipitation on the Norwegian west coast at 60°N—A tale of hurricanes and an atmospheric river. *J. Geophys. Res.*, **113**, D05102, https://doi.org/10.1029/2007JD009006.

Tveito, O. E., 2002: Spatial distribution of winter temperatures in Norway related to topography and large-scale atmospheric circulation. *IAHS Publ.*, **309**, 186–194.

——, I. Bjørdal, A. O. Skjelvåg, and B. Aune, 2005: A GIS-based agro-ecological decision system based on gridded climatology. *Meteor. Appl.*, **12**, 57–68, https://doi.org/10.1017/S1350482705001490.

van der Linden, E. C., R. J. Haarsma, and G. van der Schrier, 2018: Resolution-dependence of future European soil moisture droughts. *Hydrol. Earth Syst. Sci. Discuss.*, https://doi.org/10.5194/hess-2018-226.

van Haren, R., R. J. Haarsma, H. De Vries, G. J. Van Oldenborgh, and W. Hazeleger, 2015: Resolution dependence of circulation forced future central European summer drying. *Environ. Res. Lett.*, **10**, 055002, https://doi.org/10.1088/1748-9326/10/5/055002.

Vannforeningen, 2018: Drought and floods in 2018 – Is this climate change? (in Norwegian). Vannforeningen, https://vannforeningen.no/torke-og-%ef%ac%82om-i-2018-er-det-klimaendringer/.

van Vuuren, D. P., and Coauthors, 2011: The representative concentration pathways: An overview. *Climatic Change*, **109**, 5, https://doi.org/10.1007/S10584-011-0148-Z.

Vormoor, K., D. Lawrence, L. Schlichting, D. Wilson, and W. K. Wong, 2016: Evidence for changes in the magnitude and frequency of 70 observed rainfall vs. snowmelt driven floods in Norway. *J. Hydrol.*, **538**, 33–48, https://doi.org/10.1016/j.jhydrol.2016.03.066.

Whan, K., J. Sillmann, N. Schaller, and R. Haarsma, 2020: Future changes in atmospheric rivers and extreme precipitation in Norway. *Climate Dyn.*, **54**, 2071–2084, https://doi.org/10.1007/s00382-019-05099-z.

Zhu, Y., and R. E. Newell, 1998: A proposed algorithm for moisture fluxes from atmospheric rivers. *Mon. Wea. Rev.*, **126**, 725–735, https://doi.org/10.1175/1520-0493(1998)126<0725:APAFMF>2.0.CO;2.